

Squeezing a Prism into a Surface: Emulating Bulk Optics with Achromatic Metasurfaces

Odysseas Tsilipakos, Maria Kafesaki, Eleftherios N. Economou, Costas M. Soukoulis, and Thomas Koschny*

Metasurfaces promise to replace bulky prisms and lenses with 2D surfaces, revolutionizing wavefront control with technologically significant advantages in size, weight, and planar fabrication. However, conventional implementations suffer from large chromatic aberrations and cannot sustain performance over practical bandwidths of real-world signals because of the limited phase modulation margin available in a surface. How can an infinitely thin surface generate the arbitrarily large, broadband phase delay that bulk phase accumulation can provide? Here, equivalence between bulk optics and certain multiresonant metasurfaces is demonstrated, where phase delay arises from trains of multiple resonances in the effective sheet conductivities of the surface itself instead of accumulation of propagation phase. The fundamentally required electromagnetic surface conductivities of a purely achromatic metasurface are derived and general design rules for arbitrarily broadband beam steering and lensing are obtained. Both operation in transmission and reflection can be achieved in a unified way by proper alignment of the resonances, enabling 360° directionality. The arbitrary spectral bandwidth, dual reflection/transmission operation, and complete dispensability of propagation phase constitute a major advance in the state of the art of achromatic metasurfaces for wavefront manipulation.

1. Introduction

Metasurfaces (MSs) are ultrathin meta-material structures typically formed by periodically arranging subwavelength resonant building blocks (meta-atoms) on a 2D lattice.^[1–3] Despite their sub-wavelength thickness, they can impose a nontrivial phase discontinuity on an impinging electromagnetic wave. Spatially modulating this phase discontinuity along the metasurface unlocks the possibility of performing wavefront manipulation operations such as steering, focusing, or beam transformation. Following the formulation of the generalized Snell's law,^[4] this realization spurred a surge of research activity which consolidated into the thriving research field of gradient or graded metasurfaces.^[5–7]

In recent years, a vast range of gradient wavefront manipulation metasurfaces has been proposed in the literature, based on metallic^[8–10] or dielectric^[11–13] meta-atoms, making use of the Huygens' principle^[8,11,14] or the Pancharatnam–Berry


phase,^[4] and operating in diverse frequency regimes ranging from microwaves to the visible. These metasurfaces hold the promise of replacing conventional bulky optical components such as lenses, prisms, and gratings, thus revolutionizing wavefront control by offering significant technological advantages in size, weight, and planar fabrication. However, conventional implementations of gradient metasurfaces are typically narrow-band and cannot sustain their performance over practical spectral bandwidths. While this works for academic examples of single-plane-wave scattering, it fails to perform well for real-world signals such as modulated beams, pulses, and optical readouts, which necessarily have significant temporal and spatial bandwidth. This shortcoming is because such metasurfaces function based on the phase delay arising from the scattering by discrete meta-atom resonances, which are inherently dispersive. In contrast, classical prisms and lenses derive their optical properties from the phase accumulation via propagation inside a (variable) finite-thickness material, for which noticeable material dispersion is neither required nor desirable. As a result, researchers have very recently focused on the search for achromatic gradient metasurfaces that retain their functionality over broad spectral bandwidths and are thus suitable for practical applications.^[15–23]

Dr. O. Tsilipakos, Dr. M. Kafesaki, Prof. E. N. Economou,
Prof. C. M. Soukoulis
Institute of Electronic Structure and Laser
Foundation for Research and Technology - Hellas (FORTH-IESL)
Heraklion, Crete GR-70013, Greece
E-mail: otsilipakos@iesl.forth.gr

Dr. M. Kafesaki
Department of Materials Science and Technology
University of Crete
Heraklion, Crete GR-70013, Greece

Prof. E. N. Economou
Department of Physics
University of Crete
Heraklion, Crete GR-70013, Greece

Prof. C. M. Soukoulis, Dr. T. Koschny
Ames Laboratory—U.S. DOE and Department of Physics and Astronomy
Iowa State University
Ames, Iowa 50011, USA

 The ORCID identification number(s) for the author(s) of this article can be found under <https://doi.org/10.1002/adom.202000942>.

© 2020 The Authors. Published by Wiley-VCH GmbH. This is an open access article under the terms of the Creative Commons Attribution License, which permits use, distribution and reproduction in any medium, provided the original work is properly cited.

DOI: 10.1002/adom.202000942

Physically, it is possible to “stitch together” two arbitrary optical fields across the interface between two half-spaces if we control the distribution of the electric and magnetic current densities in this boundary (see refs. [6,14]). Consequently, we can formally emulate the exterior optical fields in regions separated by a slab, a wedge, or a lens using a single boundary that carries appropriate electric and magnetic sheet current distributions. These sheet current distributions can be implemented by a metasurface which exhibits corresponding electric and magnetic complex sheet conductivities. This raises the question: How can an infinitely thin, surface generate the arbitrarily large phase delay corresponding to an arbitrarily thick non-dispersive bulk region of space? Here, we show that we can substitute bulk phase by appropriately spaced trains of electric and magnetic resonances in the surface conductivities. Thus, we trade-off the complex spatial geometry of a trivially dispersive bulk medium for the spatial simplicity (and compactness) of a surface with complex multiresonant dispersive response, establishing a generic and powerful analogy between 2D and 3D photonic systems and paving the way to unprecedentedly thin and light optical components.

In this work, we address the fundamental question of defining the required surface electric and magnetic conductivities of a purely achromatic wavefront manipulation metasurface that can operate across arbitrarily-broad bandwidths. We derive general design rules for achieving achromatic steering and lensing operations based on implementing multiple electric and magnetic Lorentzian resonances on a single surface. The required phase delay is solely provided by the resonances implemented on the surface itself, unlike other approaches in the literature,^[17,19–21] which rely by design on the accumulation

of propagation phase in vertical waveguide segments with engineered cross-sections and consequently require a non-negligible thickness. Thus, the proposed surfaces are essentially 2D, apart from a small finite thickness to allow for implementing magnetic polarizability without magnetic materials. In addition, we treat operation in transmission and reflection in a unified way, avoiding the customary use of a metallic back-plane for reflection operation which precludes transmission altogether. We show that the proposed multiresonant metasurfaces can be configured to operate in either reflection or transmission mode, by spectrally interleaving (antimatching) or overlapping (matching) the electric and magnetic resonances, respectively. As a result, complete coverage in the entire space can be provided across the full operational bandwidth and without making any assumption about the polarization state of incident radiation. This is markedly different from recent attempts to cover operation in the entire space by either relying on different polarization states for reflection and transmission, respectively,^[24,25] or performing the operation for different wavelengths.^[26]

2. Results

Figure 1 summarizes the conceptual elements of this work. A metasurface designed to impose a specific spatially modulated group delay $\tau_g(r) = \partial_\omega \phi(r, \omega)$ can emulate the purely achromatic beam steering (focusing) performance of a fictitious bulk dielectric prism (lens) with negligible material dispersion, as illustrated in Figure 1a. Such an achromatic metasurface, besides being ultrathin and technologically advantageous, would

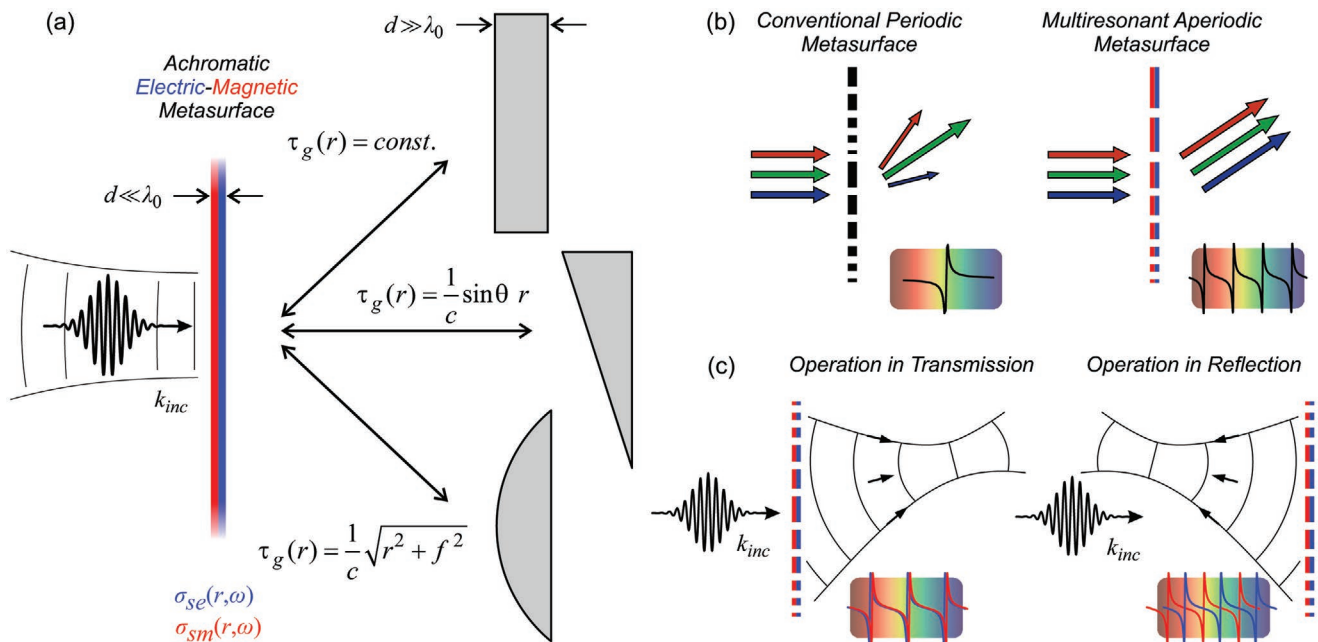


Figure 1. Metasurfaces for achromatic wavefront manipulation. a) Achromatic metasurfaces for beam deflection and focusing by properly designing the spatial profile of the imposed group delay. The steering (focusing) metasurface is a 2D equivalent of a 3D bulk dielectric prism (lens) with negligible material dispersion. σ_{se} and σ_{sm} denote the complex surface conductivities (see text and Supporting Information). b) Comparison of conventional periodic gradient metasurface with achromatic aperiodic metasurface performance for a broadband input signal. In the first case, notice the chromatic dispersion and wavelength filtering; in the second, broadband and dispersionless operation is achieved. c) Operation in transmission or reflection by spectrally overlapping the resonant electric and magnetic responses or interleaving them, respectively, as schematically shown in the insets.

additionally be favorable over an actual refractive optical component which suffers from chromatic dispersion and chromatic aberrations due to the refractive index changing with frequency, that is, material dispersion.

Furthermore, as schematically shown in Figure 1b, it significantly outperforms conventional steering metasurfaces which are periodic systems with engineered supercells that promote a single diffraction order and perfectly suppress all others only for a single operating wavelength. Such metasurfaces typically harness the phase delay of a single resonance or resonance pair; thus, the available phase span is limited to 2π , which constitutes the main obstacle toward broadband operation as will be shown below. They suffer from significant dispersion (e.g., the deflection angle varying with frequency) and low efficiency when coupling to non-desirable diffraction orders cannot be effectively suppressed. On the contrary, the proposed achromatic metasurfaces harness the phase delay offered by multiple resonances (see inset in Figure 1b); the available phase span greatly exceeds 2π enabling large group delays and allowing for an aperiodic metasurface that can be completely achromatic.

The proposed achromatic metasurfaces are both electrically and magnetically polarizable to enable unidirectional scattering (forward or backward). By spectrally overlapping (matching) or interleaving (antimatching) the resonant electric and magnetic surface conductivities σ_{se} and σ_{sm} ,^[27] they can operate in either transmission or reflection mode, allowing for covering the space both in front and back of the metasurface (see Figure 1c). The complex conductivities σ_{se} and σ_{sm} (measured in units of S and Ω , respectively) are associated with the induced surface current densities \mathbf{J}_{se} and \mathbf{J}_{sm} with units of A m^{-1} and V m^{-1} , respectively. When no magnetic materials are present, (artificial) magnetic currents are associated with the formation of electric current loops. The dimensionless counterparts of the conductivities are marked with a tilde. For details see the Supporting Information.

2.1. Theory of Achromatic Multiresonant Metasurfaces

In its most general form, a broadband achromatic metasurface must satisfy a phase compensation requirement at every frequency. Without loss of generality, we next examine the case of beam deflection in transmission from an angle θ_{in} to an angle θ_{out} . As a simple and physically intuitive ray-optics approach indicates, the distribution of phase compensation by the metasurface should be

$$\varphi(r, \omega) = \frac{\omega}{c} (\sin \theta_{out} - \sin \theta_{in}) r \quad (1)$$

where ω is the angular frequency (in rad s^{-1}), c is the speed of light, and r is the position on the metasurface. Note that Equation (1) is linear in ω . In contrast, the phase response stemming from a single Lorentzian resonance is inherently dispersive, revealing why conventional gradient metasurfaces can only satisfy Equation (1) for a central design frequency ω_0 . In addition, Equation (1) indicates that large phase and group delays are required especially for covering high deflection angles and large metasurface extents, necessitating the

exploitation of multiple resonances. Finally, achromatic metasurfaces can no longer be periodic, as also highlighted in refs. [15,22], because the required periodicity D would have to be different for each operating wavelength, λ , according to $\varphi(r + D, \omega) = \varphi(r, \omega) + m2\pi \Rightarrow D = m\lambda/\Delta_{\sin}$. Δ_{\sin} denotes the difference $\sin \theta_{out} - \sin \theta_{in}$.

Very recently, we have proposed uniform metasurfaces supporting multiple Lorentzian resonances in the surface conductivities that can supply phase discontinuities greatly exceeding 2π over broad bandwidths and can exhibit a phase profile exactly linear in frequency ($\varphi(\omega) \propto \omega$) leading to a spectrally constant group delay.^[28,29] Such metasurfaces were exploited for delaying broadband pulses without any pulse distortion and can work in either reflection^[28] or transmission.^[29] The aforementioned traits are exactly those required by Equation (1), as seen by taking the derivative with respect to the angular frequency. The required group delay τ_g for an achromatic beam deflection metasurface is

$$\tau_g(r) = \frac{\sin \theta_{out}}{c} r \quad (2)$$

where we have assumed normal incidence, that is, $\theta_{in} = 0$. The group delay is spectrally constant but spatially modulated, as schematically shown in Figure 2a. The spatial modulation of the required group delay can be realized by the denser or sparser frequency packing of the resonances. The surface conductivities that implement the required group delay profile are given by (see the Supporting Information)

$$\tilde{\sigma}_{se}(r) = \frac{1 \pm \mathcal{A} e^{i\tau_g(r)\omega}}{1 \mp \mathcal{A} e^{i\tau_g(r)\omega}} = \tilde{\sigma}_{sm}(r) \quad (3)$$

where operation in transmission has been assumed, $\tilde{\sigma}_{se} = \tilde{\sigma}_{sm}$, and \mathcal{A} allows for some absorption in the metasurface ($\mathcal{A} \leq 1$) in line with actual physical realizations. The target spectrum of Equation (3) can be excellently approximated with trains of physically realizable Lorentzian resonances with resonance frequencies $\omega_k(r) = \{[(2k+1)\pi]^2 + \ln^2(\mathcal{A})\}^{1/2} / \tau_g(r)$ with $k = 0, 1, 2, \dots$ or $\omega_k(r) = \{(2k\pi)^2 + \ln^2(\mathcal{A})\}^{1/2} / \tau_g(r)$ with $k = 0, 1, 2, \dots$ depending on the sign selection in Equation (3). Each resonance is by itself bandwidth limited, but combining multiple resonances into an aggregate bandwidth of high reflection/transmission allows to greatly extend the operational bandwidth (up to arbitrary extents) and at the same time operate with large time delays dictated by the quality factor^[30] of the constituent resonances. More information on the multiresonant prescription for achromatic wavefront manipulation can be found in the Supporting Information.

As an example, the required dimensionless electric surface conductivity on the metasurface (imaginary part) for an output angle $\theta_{out} = 30^\circ$ (assuming normal incidence) is plotted in Figure 2b as a function of normalized frequency (ω/ω_0) and normalized position on the metasurface (r/λ_0), where $\omega_0(\lambda_0)$ is the center design frequency(wavelength). For operation in transmission the magnetic conductivity is simply $\tilde{\sigma}_{sm} = \tilde{\sigma}_{se}$, whereas for operation in reflection $\tilde{\sigma}_{sm} = 1/\tilde{\sigma}_{se}$.^[28] The cut along frequency highlights the multiresonant nature of the required metasurface; for $r/\lambda_0 = 10$ three electric resonances are needed (plus three magnetic) in the frequency range $0.75\omega_0 - 1.25\omega_0$. The

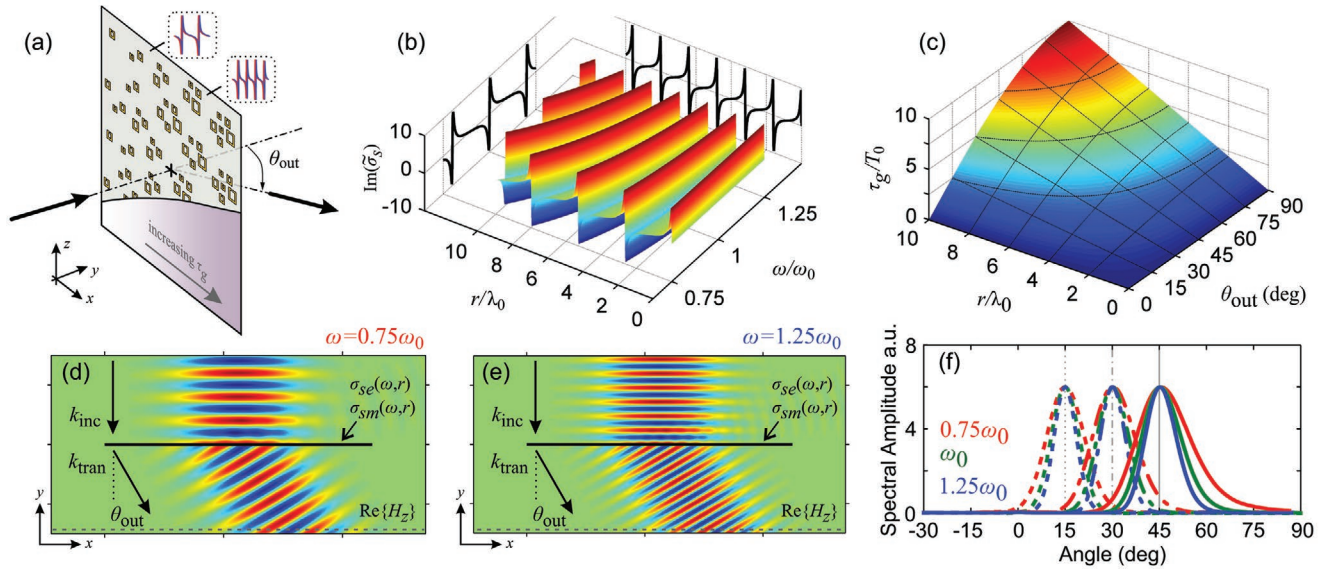


Figure 2. Prescription and performance of multiresonant achromatic metasurface for beam steering. a) Schematic illustrating the increase in required group delay along the metasurface by the denser packing of resonances. b) Required resonant electric surface conductivity (imaginary part) for $\theta_{\text{out}} = 30^\circ$ assuming normal incidence. The dimensionless electric conductivity $\tilde{\sigma}_{se}$ is plotted. The magnetic conductivity is given by $\tilde{\sigma}_{sm} = \tilde{\sigma}_{se}$ for transmission or $\tilde{\sigma}_{sm} = 1/\tilde{\sigma}_{se}$ for reflection. c) Required group delay as a function of position on the metasurface and desired deflection angle θ_{out} assuming normal incidence. d–e) Field distributions ($\text{Re}\{H_z\}$) of beam steering in transmission for $\theta_{\text{in}} = 0$ and $\theta_{\text{out}} = 30^\circ$. Two different frequencies are shown ($0.75\omega_0$, $1.25\omega_0$) spanning a range of 50% about the central frequency. f) Angular content of output beams for $\omega = 0.75\omega_0$, ω_0 , and $1.25\omega_0$ and $\theta_{\text{out}} = 15^\circ, 30^\circ, 45^\circ$.

required group delay on the metasurface as a function of desired deflection angle is depicted in Figure 2c. It is normalized with respect to the carrier cycle of the central frequency $T_0 = 1/f_0$. The required group delay increases with deflection angle and with position on the metasurface; the latter can be also verified by the denser packing of resonances that is required with increasing r in Figure 2b. For $r/\lambda_0 = 10$ and a moderate deflection angle of 30° , the required group delay is $5T_0$.

Finally, note that the prescription of a spatially linear phase given by Equation (1) is based on a ray-optics (or phase-shift as also commonly termed^[6]) approach. It is known that this approach is prone to spurious diffraction and lower efficiency as Δ_{sin} increases because the input and output impedance cannot be concomitantly matched.^[31] Following an approach based on stipulating the desired fields above and below the deflection metasurface and applying the boundary conditions (a procedure commonly termed surface-impedance approach^[6]), it has been shown that the exact solution would require surface conductivities with locally active regions or, equivalently, spatial dispersion.^[31,32] Besides the local amplitude variation including values exceeding unity, the associated phase profile deviates from being linear, especially as the deflection angle increases.^[33] For a connection between the ray-optics and the surface-impedance approach see the Supporting Information. In this work, since we are interesting in establishing an achromatic response over arbitrarily broad spectral bandwidths and not obtaining maximum efficiency even for grazing angles, we work with Equation (1).

2.2. Performance Analysis

The achromatic performance of the proposed multiresonant metasurfaces is demonstrated in Figure 2. We consider

a steering example in transmission for a Gaussian beam with a waist radius of $3\lambda_0$ taking place at the position of the metasurface (λ_0 is a central operating wavelength). A finite metasurface of extent $15\lambda_0$ is assumed to fully accommodate the beam avoiding edge diffraction effects and the associated intensity ripples.^[34] We perform rigorous full-wave electromagnetic simulations with COMSOL Multiphysics, assuming an abstract metasurface with the prescribed electric and magnetic complex conductivities, $\sigma_{se}(\omega, r)$ and $\sigma_{sm}(\omega, r)$, implemented as electric and magnetic current boundary conditions, respectively. The required $\sigma_{se}(\omega, r)$ and $\sigma_{sm}(\omega, r)$ of Equation (3) have been approximated as a train of Lorentzian resonances to be physically realizable (see the Supporting Information).

In Figure 2d,e the polarization of the incident beam lies inside the xy incidence plane and we plot the $\text{Re}\{H_z\}$ field distribution for two operating frequencies, $0.75\omega_0$ and $1.25\omega_0$, spanning a vast, 50% range about the central frequency ω_0 (for comparison, such a range roughly corresponds to the bandwidth of visible light). Excellent steering performance to the designated output angle of 30° is achieved for all frequencies. This is quantitatively verified in Figure 2f, depicting the angular spectrum of the output beams (dash-dot lines) for three operating frequencies $0.75\omega_0$, ω_0 , and $1.25\omega_0$. The output plane where the Fourier transform is calculated is marked in Figure 2d,e with a dashed gray line. The peak of the output spectrum is exactly centered at 30° for all three operating frequencies. The different linewidths for the three frequencies is because the same k_{\parallel} content corresponds to a different angular content through $k_{\parallel} = k \sin(\theta_{\text{out}})$. This reflects that given the same waist extent, beams of lower frequency are bound to spread more during propagation, as anticipated.

Additional steering scenarios for $\theta_{\text{out}} = 15^\circ$ and 45° are also examined in Figure 2f. In all cases, the peak is found at the prescribed angle and no spurious diffraction is observed. Notice that for each frequency, as the deflection angle increases the spectral linewidth increases as well, indicating a larger tendency for beam broadening since plane waves deviating more from the central direction are involved. This is because the effective waist size of the output beam w'_0 is smaller than the input one according to $w'_0 = w_0 \cos(\theta_{\text{out}})$. As a result, the Rayleigh distance $z_R = \pi(w'_0)^2/\lambda$ at which the beam spreads by a factor of $\sqrt{2}$ decreases as well. This modification of the output beam waist is because the change of beam direction happens on the same planar surface (see the Supporting Information). For the most extreme case in Figure 2a of $\theta_{\text{out}} = 45^\circ$ and $\omega = 0.75\omega_0$ the Rayleigh distance is only $\sim 5.65\lambda_0$. Since we are discussing tightly focused beams ($w_0 = 3\lambda_0$), diffraction along propagation can become relevant even for relatively small distances, especially as the deflection angle increases. Further examples of beam steering performance involving deflection angles ranging up to 75° can be found in the Supporting Information.

Finally, note that the steering metasurface is designed to supply a specific parallel wavevector contribution $k_{\parallel}^{\text{surf}} = k\Delta_{\text{sin}}$ for each frequency (Equation (1)). When the incidence angle changes significantly from the prescribed, beam deflection operation is preserved but the output angle changes as dictated by momentum conservation $k_{\parallel}^{\text{out}} = k_{\parallel}^{\text{in}} + k_{\parallel}^{\text{surf}}$ (see Supporting Information).

2.3. Effect of the Discrete Nature of Meta-Atoms

Toward practical physical implementation, we next investigate a discretized version of the proposed metasurface for achromatic steering. It consists of strips corresponding to different group delay values (Figure 3a). Each strip has width d and the surface conductivities are assumed piece-wise con-

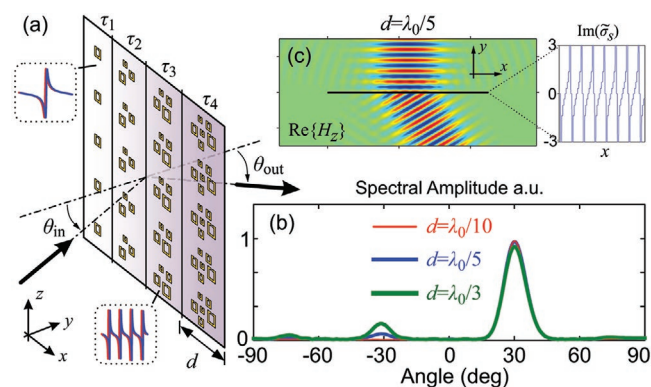


Figure 3. Discretized version of multiresonant achromatic metasurface. a) Schematic showing discrete meta-atoms arranged in strips of width d . b) Output beam spectrum as d changes for a steering scenario in transmission at operating frequency ω_0 with $\theta_{\text{in}} = 0$ and $\theta_{\text{out}} = 30^\circ$. Only for very coarse discretization of the required conductivity profile, spurious diffraction lobes start to appear. c) Field distribution for $d = \lambda_0/5$. The piece-wise constant approximation of the required surface conductivity is shown in the inset.

stant across them. We consider a steering scenario in transmission at operating frequency ω_0 with $\theta_{\text{in}} = 0$ and $\theta_{\text{out}} = 30^\circ$. The output beam spectrum is depicted in Figure 3b for the cases $d = \lambda_0/10$, $\lambda_0/5$ and $d = \lambda_0/3$. For $d = \lambda_0/10$, it is indistinguishable from the continuous case. It is only for coarse discretizations of the surface conductivity that spurious diffraction lobes start to appear. More specifically, the period of the conductivity profile at frequency ω equals $\lambda/\Delta_{\text{sin}} = 2\lambda$. This means that diffraction channels at angles -30° , 0° , 30° are open and those at -90° , 90° are in the limit of becoming propagating; these diffraction angles are constant for all frequencies demonstrating the achromaticity of the metasurface even in the spurious diffraction orders. Discretization compromises the surface conductivity prescription and some power couples mainly to the -30° available diffraction channel as seen in Figure 3b. There is also some power coupled to available reflection diffraction orders (see the Supporting Information). If the steering scenario changes to, for example, $\theta_{\text{out}} = 45^\circ$, the spurious lobes now appear around -45° and 0° as dictated by the $\lambda/\Delta_{\text{sin}}$ periodicity (see Supporting Information).

2.4. Truncating the Infinite Lorentzian Sum

The initial prescription for the realization of achromatic steering requires infinite trains of Lorentzian resonances in the electric (and magnetic) surface conductivities. Truncating the Lorentzian sums makes the recipe more amenable to practical realization. Depending on the frequency range of interest and the extent of the metasurface, a different number of resonances becomes relevant. For the particularly wide-band scenario $\omega = 0.75\omega_0 - 1.25\omega_0$ and assuming $r_{\text{max}} = 15\lambda_0$, keeping 10 (+10) resonances results in indistinguishable performance with respect to the untruncated case. In Figure 4, a beam steering example from $\theta_{\text{in}} = 0$ to $\theta_{\text{out}} = 30^\circ$ is examined keeping 5 (+5) resonances to allow for a good approximation of the target spectrum for a broad range of frequencies. Even with a crude sum truncation, that is, by just omitting lower and higher order terms, we can get good approximation of the ideal transmission phase and amplitude of the untruncated recipe (Figure 4a,b). The resulting steering behavior is very good as verified by the planar wavefronts along 30° in the inset of Figure 4b. Even better performance can be achieved by more elaborate truncation, that is, by fine tuning the characteristics of the involved resonances (frequency, strength, and damping) to account for and counteract the effects of truncation.

2.5. Broadband Beam Focusing

The multiresonant achromatic approach can be applied to achieve practically any wavefront manipulation operation. Besides beam steering, a prominent example of wavefront control is lensing or focusing. In this case, the group delay profile should satisfy $\tau_g(r) = \sqrt{(r^2 + f_{\text{des}}^2)}/c$, where f_{des} is the designated focal distance; the resulting metasurface can then emulate the response of a bulk lens, Figure 1a.

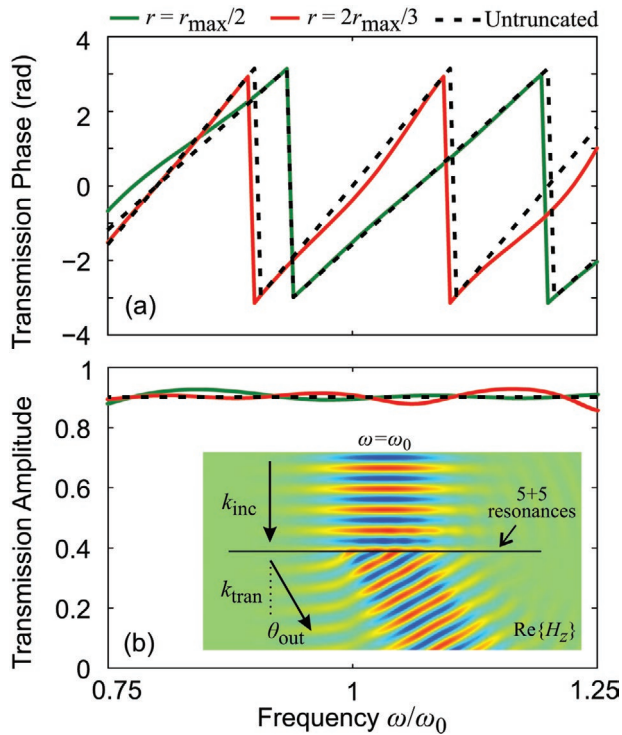


Figure 4. Truncated recipe for achromatic steering to $\theta_{\text{out}} = 30^\circ$ involving 5 electric and 5 magnetic resonances. Transmission phase (a) and amplitude (b) at different positions on the metasurface: $r = r_{\max}/2$ and $r = 2r_{\max}/3$ with $r_{\max} = 15\lambda_0$. Inset: field distribution of beam steering ($\text{Re}\{H_z\}$) for an operating frequency $\omega = \omega_0$.

In **Figure 5**, we demonstrate an example of short-profile beam focusing with a designated focal distance $f_{\text{des}} = 3\lambda_0$; a distinct advantage of metasurface-based lenses that enable producing focal spots at ultrashort distances from the flat lensing component. This time, we opt for operation in reflection by implementing the antimatching condition $\tilde{\sigma}_{sm} = 1/\tilde{\sigma}_{se}$. Figure 5a depicts the scattered field distribution for an operating frequency $\omega = \omega_0$, showing a clear focal spot. The same performance is observed for operating frequencies $0.75\omega_0$ and $1.25\omega_0$ (Supporting Information). The actual focal distance in Figure 5a is $f_{\text{act}} = 2.9\lambda_0$ almost in perfect agreement with f_{des} . Note that the prescribed group delay referred to a plane wave excitation with a single k component, and not the actual Gaussian beam,^[35] explaining this small discrepancy between f_{act} and f_{des} .

In Figure 5b, we examine additional focusing scenarios for $f_{\text{des}} = 2\lambda_0, 3\lambda_0, \dots, 8\lambda_0$ and operating frequencies $\omega = 0.75\omega_0, \omega_0, 1.25\omega_0$. For all cases the actual focal distance is found in very good agreement with the designated value. In Figure 5c, we plot the spot size by calculating the amplitude full-width half maximum (FWHM) normalized to the operating wavelength. As f_{des} increases, the numerical aperture decreases and the spot size starts to increase. The performance is identical for all operating frequencies. A wider incident Gaussian beam (currently the waist radius is only $3\lambda_0$) would feature smaller spot sizes for the same designated focal distances.

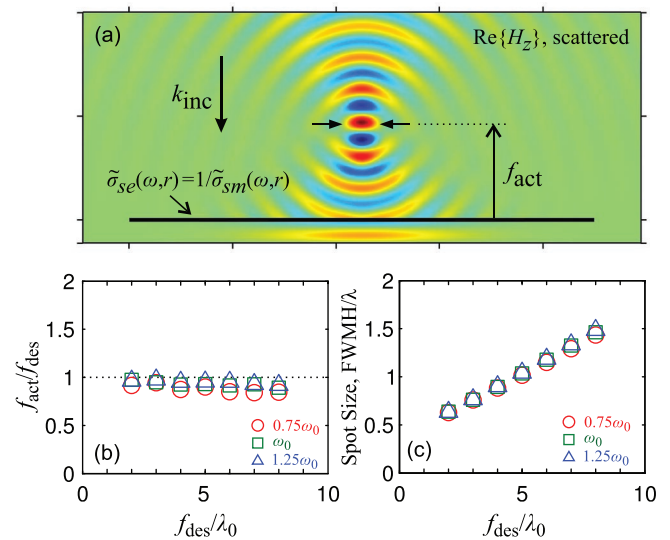


Figure 5. Performance of multiresonant achromatic metasurface for focusing in reflection mode. a) Scattered field distribution for a designated focal distance $f_{\text{des}} = 3\lambda_0$ and an operating frequency $\omega = \omega_0$. b) Actual focal distance f_{act} for different designated focal distances, indicating excellent performance for all three frequencies. c) Focal spot size as a function of f_{des} ; the amplitude full-width half maximum (FWHM) of the spot at the actual focal plane is plotted normalized to the operating wavelength. As f_{des} increases, the numerical aperture decreases and the spot size starts to increase.

2.6. Feasibility of Physical Implementation

Here, we present a preliminary physical implementation example of the multiresonant unit cell, serving as a feasibility verification of the proposed achromatic metasurface concept. We use metallic meta-atoms and specifically electric-LC resonators (ELCs) and split ring resonators (SRRs) for implementing the electric and magnetic resonances, respectively (**Figure 6a**). For more details on the design, see the Supporting Information. The example is targeted for microwave frequencies where metals feature low loss. We manage to fit five resonances (three electric + two magnetic) in a sub-wavelength unit cell ($d \sim \lambda_0/2$). The resonances are spectrally interleaved targeting operation in reflection (Figure 6b). The dimensionless electric and magnetic surface conductivities are plotted as retrieved from the complex plane-wave scattering coefficients,^[28] obtained from full wave simulations. The achieved group delay is equal to 1.5 ns and fairly constant (less than 15% peak to peak ripple) across a broad bandwidth of 860 MHz about the central frequency $f_0 = 11$ GHz ($T_0 = 0.091$ ns); this amounts to $\tau_g/T_0 \approx 16.5$ exceeding the requirements in Figure 2b. At the same time, the reflection amplitude is high and flat across the said bandwidth (see the Supporting Information). As mentioned previously, by spectrally positioning the Lorentzian resonances further apart, the achieved group delay can be decreased so as to provide the spatial modulation along the metasurface that is required. Importantly, note that the thickness of the structure can be deeply subwavelength, since the phase delay is solely originating from the implemented resonances and not

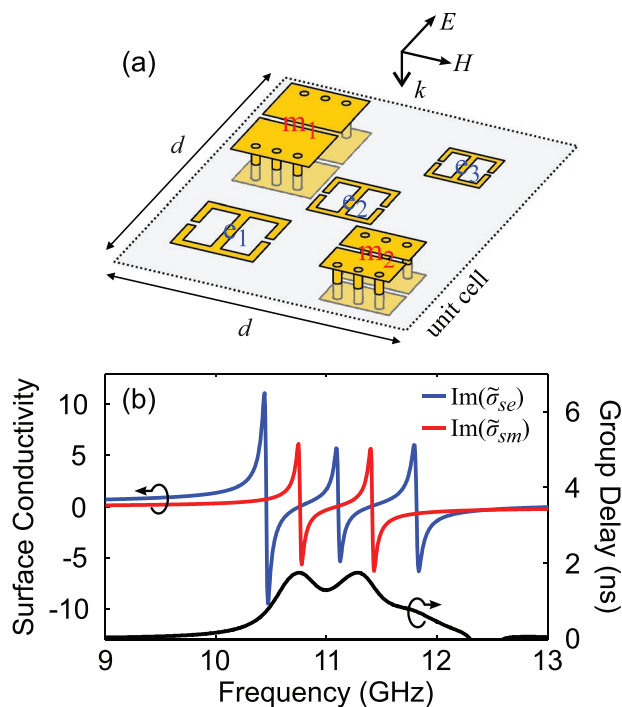


Figure 6. a) Example of multiresonant unit cell for a microwave implementation of the proposed concept, based on electric-LC meta-atoms and split ring resonators for the electric and magnetic resonances, respectively. b) Resulting Lorentzian resonances (three electric plus two magnetic) in the surface conductivities, spectrally interleaved for operation in reflection. The achieved group delay equals 1.5 ns ($\tau_g/T_0 \approx 16.5$) and is fairly constant across a bandwidth of 860 MHz about the central frequency $f_0 = 11$ GHz.

phase accumulation. In this example, $h = 3.7$ mm $\approx \lambda_0/8$, equal to the height of the magnetic resonator (a finite thickness is required for magnetic polarizability). This is markedly different from implementations based on waveguide segments^[17,19–21] which harness the required group delay from propagation along the height H of these segments ($\tau_g(r) = H/v_g(r)$), thus posing a corresponding limit on the structure thickness of $H \geq 10\lambda_0/n_g$, assuming a requirement of $\tau_g = 10T_0$ according to Figure 2c.

3. Discussion and Conclusions

We have derived fundamental design rules for realizing achromatic wavefront manipulation metasurfaces based solely on resonant phase delay, by implementing trains of Lorentzian resonances in the electric and magnetic surface conductivities, emulating the bulk phase accumulation that lends functionality to classical optical devices. The advantage of this approach is that it can lead to ultrathin realizations, since it does not require accumulation of propagation phase. In addition, we treat operation in both transmission and reflection mode in a unified way, by spectrally shifting the electric and magnetic resonances with respect to each other (overlapping vs interleaved), avoiding the use of a metallic backplane for reflection as customarily exercised. Directionality of 360°

can, thus, be achieved overcoming a long-standing limitation of gradient metasurfaces. Applying the derived rules, we have demonstrated achromatic beam-steering and focusing, which extend to theoretically arbitrary bandwidths. To demonstrate the practical feasibility of the proposed approach, a concrete, ultrathin ($\approx \lambda_0/8$) physical implementation example of a multiresonant unit cell based on metallic meta-atoms for operation in the microwave regime has been proposed and numerically demonstrated.

Fundamentally, our work shows how broadband conventional 3D optical components such as prisms and lenses can be “squeezed” into equivalent 2D surfaces by replacing the phase delay caused by accumulation of propagation phase across the bulk medium with the arbitrarily large phase delay arising from specific trains of multiple resonances in the effective sheet conductivities of the surface itself. This establishes a generic and powerful analogy between 2D and 3D photonic systems and paves the way to thinner and lighter optical components.

In conclusion, our work addresses current bottlenecks and limitations in the theory and design of achromatic metasurfaces and can lead to advantageous implementations of achromatic flat optical components. Achromatic operation across arbitrarily broad spectral bandwidths, essentially infinitesimally thin optical components made possible by the complete dispensability of bulk propagation phase, and dual reflection/transmission operation enabling 360° coverage, are important properties that constitute a major advance in the state of the art of achromatic metasurfaces for wavefront manipulation.

Supporting Information

Supporting Information is available from the Wiley Online Library or from the author.

Acknowledgements

Work at Ames Laboratory was supported by the Department of Energy (Basic Energy Sciences, Division of Materials Sciences and Engineering) under Contract No. DE-AC02-07CH11358. Work at FORTH was partially supported by the European Union’s Horizon 2020 FETOPEN programme under project VISORSURF Grant Agreement No. 736876 and project NANOPOLY Grant Agreement No. 829061. O.T. acknowledges the financial support of the Stavros Niarchos Foundation within the framework of project ARCHERS.

Conflict of Interest

The authors declare no conflict of interest.

Keywords

achromatic metasurfaces, broadband, flat optics, gradient metasurfaces, multiple resonances

Received: June 10, 2020
Revised: August 27, 2020
Published online: October 1, 2020

- [1] S. B. Glybovski, S. A. Tretyakov, P. A. Belov, Y. S. Kivshar, C. R. Simovski, *Phys. Rep.* **2016**, 634, 1.
- [2] H.-T. Chen, A. J. Taylor, N. Yu, *Rep. Prog. Phys.* **2016**, 79, 076401.
- [3] O. Tsilipakos, A. C. Tasolamprou, A. Ptilakis, F. Liu, X. Wang, M. S. Mirmoosa, D. C. Tzarouchis, S. Abadal, H. Taghvaei, C. Liaskos, A. Tsioliariidou, J. Georgiou, A. Cabellos-Aparicio, E. Alarcón, S. Ioannidis, A. Pitsillides, I. F. Akyildiz, N. V. Kantartzis, E. N. Economou, C. M. Soukoulis, M. Kafesaki, S. Tretyakov, *Adv. Opt. Mater.* **2020**, 8, 2000783.
- [4] N. Yu, P. Genevet, M. A. Kats, F. Aieta, J.-P. Tetienne, F. Capasso, Z. Gaburro, *Science* **2011**, 334, 333.
- [5] N. M. Estakhri, A. Alù, *J. Opt. Soc. Am. B* **2016**, 33, A21.
- [6] A. Epstein, G. V. Eleftheriades, *J. Opt. Soc. Am. B* **2016**, 33, A31.
- [7] F. Ding, A. Pors, S. I. Bozhevolnyi, *Rep. Prog. Phys.* **2018**, 81, 026401.
- [8] C. Pfeiffer, A. Grbic, *Phys. Rev. Lett.* **2013**, 110, 197401.
- [9] V. S. Asadchy, Y. Ra'di, J. Vehmas, S. A. Tretyakov, *Phys. Rev. Lett.* **2015**, 114, 095503.
- [10] F. Liu, O. Tsilipakos, A. Ptilakis, A. C. Tasolamprou, M. S. Mirmoosa, N. V. Kantartzis, D.-H. Kwon, J. Georgiou, K. Kossifos, M. A. Antoniadis, M. Kafesaki, C. M. Soukoulis, S. A. Tretyakov, *Phys. Rev. Appl.* **2019**, 11, 044024.
- [11] M. Decker, I. Staude, M. Falkner, J. Dominguez, D. N. Neshev, I. Brener, T. Pertsch, Y. S. Kivshar, *Adv. Opt. Mater.* **2015**, 3, 813.
- [12] Y. F. Yu, A. Y. Zhu, R. Paniagua-Domínguez, Y. H. Fu, B. Luk'yanchuk, A. I. Kuznetsov, *Laser Photonics Rev.* **2015**, 9, 412.
- [13] O. Tsilipakos, A. C. Tasolamprou, T. Koschny, M. Kafesaki, E. N. Economou, C. M. Soukoulis, *Adv. Opt. Mater.* **2018**, 6, 1800633.
- [14] M. Selvanayagam, G. V. Eleftheriades, *Opt. Express* **2013**, 21, 14409.
- [15] F. Aieta, M. A. Kats, P. Genevet, F. Capasso, *Science* **2015**, 347, 1342.
- [16] S. M. A. M. H. Abadi, K. Ghaemi, N. Behdad, *IEEE Trans. Antennas Propag.* **2015**, 63, 534.
- [17] E. Arbabi, A. Arbabi, S. M. Kamali, Y. Horie, A. Faraon, *Optica* **2017**, 4, 625.
- [18] S. Wang, P. C. Wu, V.-C. Su, Y.-C. Lai, C. Hung Chu, J.-W. Chen, S.-H. Lu, J. Chen, B. Xu, C.-H. Kuan, T. Li, S. Zhu, D. P. Tsai, *Nat. Commun.* **2017**, 8, 187.
- [19] S. Wang, P. C. Wu, V.-C. Su, Y.-C. Lai, M.-K. Chen, H. Y. Kuo, B. H. Chen, Y. H. Chen, T.-T. Huang, J.-H. Wang, R.-M. Lin, C.-H. Kuan, T. Li, Z. Wang, S. Zhu, D. P. Tsai, *Nat. Nanotechnol.* **2018**, 13, 227.
- [20] S. Shrestha, A. C. Overvig, M. Lu, A. Stein, N. Yu, *Light Sci. Appl.* **2018**, 7, 85.
- [21] W. T. Chen, A. Y. Zhu, V. Sanjeev, M. Khorasaninejad, Z. Shi, E. Lee, F. Capasso, *Nat. Nanotechnol.* **2018**, 13, 220.
- [22] A. A. Fathnan, D. A. Powell, *Opt. Express* **2018**, 26, 29440.
- [23] A. A. Fathnan, A. E. Olk, D. A. Powell, preprint arXiv:1912.03936, **2019**.
- [24] T. Cai, G. Wang, S. Tang, H. Xu, J. Duan, H. Guo, F. Guan, S. Sun, Q. He, L. Zhou, *Phys. Rev. Appl.* **2017**, 8, 034033.
- [25] H. Yi, S. Qu, K. Ng, C. K. Wong, C. H. Chan, *IEEE Trans. Antennas Propag.* **2018**, 66, 209.
- [26] A. Forouzmand, M. Salary, G. K. Shirmanesh, R. Sokhoyan, H. A. Atwater, H. Mosallaei, *Nanophotonics* **2019**, 8, 415.
- [27] P. Tassin, T. Koschny, C. M. Soukoulis, *Physica B* **2012**, 407, 4062.
- [28] O. Tsilipakos, T. Koschny, C. M. Soukoulis, *ACS Photon.* **2018**, 5, 1101.
- [29] V. Ginis, P. Tassin, T. Koschny, C. M. Soukoulis, *Appl. Phys. Lett.* **2016**, 108, 031601.
- [30] T. Christopoulos, O. Tsilipakos, G. Sinatkas, E. E. Kriezis, *Opt. Express* **2019**, 27, 14505.
- [31] A. Díaz-Rubio, V. S. Asadchy, A. Elsakka, S. A. Tretyakov, *Sci. Adv.* **2017**, 3, e1602714.
- [32] A. Epstein, G. V. Eleftheriades, *Phys. Rev. Lett.* **2016**, 117, 256103.
- [33] N. M. Estakhri, A. Alù, *Phys. Rev. X* **2016**, 6, 041008.
- [34] A. E. Siegman, *Lasers*, University Science Books, Sausalito, CA **1986**.
- [35] J. Martínez-Llinàs, C. Henry, D. Andrén, R. Verre, M. Käll, P. Tassin, *Opt. Express* **2019**, 27, 21069.